RSC Advances

PAPER

View Article Online
View Journal | View Issue

Cite this: *RSC Adv.*, 2021, **11**, 39619

Synaptic transistors based on a tyrosine-rich peptide for neuromorphic computing†

Min-Kyu Song,[a] Young-Woong Song,[a] Taehoon Sung,[a] Seok Daniel Namgung,[bd] Jeong Hyun Yoon,[a] Yoon-Sik Lee,[c] Ki Tae Nam[bd] and Jang-Yeon Kwon*[a]

In this article, we propose an artificial synaptic device based on a proton-conducting peptide material. By using the redox-active property of tyrosine, the Tyr–Tyr–Ala–Cys–Ala–Tyr–Tyr peptide film was utilized as a gate insulator that shows synaptic plasticity owing to the formation of proton electric double layers. The ion gating effects on the transfer characteristics and temporal current responses are shown. Further, timing-dependent responses, including paired-pulse facilitation, synaptic potentiation, and transition from short-term plasticity to long-term plasticity, have been demonstrated for the electrical emulation of biological synapses in the human brain. Herein, we provide a novel material platform that is bio-inspired and biocompatible for use in brain-mimetic electronic devices.

Received 28th August 2021
Accepted 29th November 2021

DOI: 10.1039/d1ra06492d

rsc.li/rsc-advances

Introduction

The recent emergence of artificial intelligence has impacted a wide range of research areas owing to its superior performance in cognitive computing including inference, decision, and prediction, which has been regarded as a human role.[1] The large amount of data and repetitive processing for training have driven increasing demands for the development of high-performance processors. However, conventional processors have parallel processing limits for cognitive computing owing to their von Neumann architecture, which has separate memory and processing units. Transferring data between them induces a considerable waste of time and power, called the von Neumann bottleneck. Neuromorphic devices have emerged to emulate human brain functions to overcome the von Neumann bottleneck.[2–6] In contrast to man-made computers, the biological brain is composed of $\sim 10^{11}$ neurons and $\sim 10^{15}$ synapses that process data locally and in parallel, thus affording extreme efficiency in terms of time and energy.[7] Synaptic devices that mimic the fundamental function of synapses have been proposed as building blocks for brain-like processors.[8–10] Several researchers have developed artificial synapses for spiking neural networks by using the timing-dependent electrical characteristics of ion-based devices to realize synaptic plasticity.[11,12] Among the various approaches, synaptic transistors are regarded as promising candidates for artificial synapses owing to their functional similarity to synapses, low power consumption, and controllability of synaptic performance.[13–16]

Peptide materials, which are short chains of amino acids, offer significant advantages for use in electronic devices as their chemical and electrical properties can be programmed by designing amino acid sequences, controlling their folding, and inducing assembly.[17–20] More importantly, they play key roles in ion transfer in biological signaling systems, implying their potential role for ion-controlling in electronics.[21] Recently, we designed a certain tyrosine-rich peptide (TRP) to show proton-conducting characteristics using tyrosine.[22–24] Introducing repeating tyrosine units at both ends of the peptide sequences enables high proton-conducting and redox-active insulating properties in thin films. In this regard, we explored the possibility of TRP materials for use in biomedical devices by utilizing their proton-mediated redox reaction as well as their biocompatibility and biodegradability, and further applicability for neuromorphic devices.[25–27]

In this letter, we report a proton-gated synaptic transistor using an In–Ga–Zn–O (IGZO) semiconducting film on a Tyr–Tyr–Ala–Cys–Ala–Tyr–Tyr (YYACAYY, Y7C) peptide thin film. The proton-conducting property of the TRP film not only enabled excellent performance with an on/off ratio of around 10^7 but also large hysteresis of the transfer curves owing to the formation of electric double layers of protons. Thus, the timing-dependent synapse-mimetic responses of the drain current modulated by gate voltage spikes are presented. Treating the device as an artificial synapse, we explored its synaptic plasticity including paired-pulse facilitation (PPF), short-term to long-term transition, and potentiation.

[a]*School of Integrated Technology, Yonsei University, Incheon 21983, Republic of Korea. E-mail: jangyeon@yonsei.ac.kr*

[b]*Department of Materials Science and Engineering, Seoul National University, Seoul 08826, Republic of Korea*

[c]*School of Chemical and Biological Engineering, Seoul National University, Seoul 08826, Republic of Korea*

[d]*Soft Foundry, Seoul National University, Seoul 08826, Republic of Korea*

† Electronic supplementary information (ESI) available. See DOI: 10.1039/d1ra06492d

Experimental section

Fabrication of the Y7C peptide synaptic transistor

4 wt% Y7C peptide powder (scipeptide, 97%) was dissolved in trifluoroacetic acid (Daejung, 99.0%). The Y7C solution was sonicated for 30 min and centrifuged at 12 000 rpm for 1 min. Before the spin-coating process, highly doped Si substrates with a resistivity of 0.001–0.005 Ω cm were cleaned *via* sonication in acetone, isopropyl alcohol, and water for 5 min per cleaner. The solution was then spin-coated onto the P^+ Si substrates at 4000 rpm for 60 s. The IGZO channel layer was patterned using a shadow mask. The lateral size of the IGZO was 400 × 400 μm. The 50 nm-thick IGZO was deposited by RF sputtering under a working pressure of 7 mTorr and an RF power of 100 W, and the gas flow rates of O_2 and Ar were 30 sccm and 0.5 sccm, respectively. A 100 nm-thick Mo source/drain layer patterned with a shadow mask was deposited by DC sputtering under a power of 200 W and an Ar gas flow rate of 30 sccm. The lateral size of the Mo electrodes was 200 × 200 μm. The channel length and width were both 200 μm. The rear side of the substrate was connected to copper tape on the glass with silver paste for the gate electrode, followed by the native oxide etching of Si.

Film characterization of the Y7C peptide

The thickness of the Y7C peptide film as a function of concentration was measured using an atomic force microscope (AFM, XE-100, Park systems). A semiconductor parameter analyzer (Keithley SCS 4200) was used for the electrical characterization. The humidity and temperature conditions were maintained at 40 ± 5% RH and 22 ± 2 °C during the measurements.

Results and discussion

Tyrosine is a redox-active amino acid known to play a key role in various enzymatic reactions in biological systems such as photosynthesis II.[21] Tyrosine transfers protons and electrons simultaneously *via* an inherent deprotonation of its phenolic hydroxyl group, known as proton-coupled electron transfer (PCET).[21,28] This phenomenon can also be observed in the TRP thin film, where protons are transported *via* phenolic hydroxyl groups as hopping sites.[24,27] Therefore, the Y7C peptide thin film exhibits high proton conductivity, in contrast to low electron conductivity. This suggests its potential for use in proton-based synaptic devices for neuromorphic applications. Thus, we fabricated an IGZO thin-film transistor with a Y7C peptide film as a gate insulator. The Y7C peptide solution was spin-coated onto a highly doped p-type Si wafer. The thickness of the Y7C film was measured by the AFM (see Fig. S1†). Fig. S2† shows the *I–V* characteristics of the insulating Y7C film. The IGZO active layer and Mo source/drain metal layers were deposited using RF sputtering and DC sputtering, respectively.

Fig. 1 shows the schematics of the Y7C peptide synaptic transistor and the corresponding biological synapse between the two neurons. In biological synapses, presynaptic stimuli from pre-neurons induce the emission of neurotransmitters such as Na^+, K^+, and dopamine to the synaptic cleft, as shown in Fig. 1a. Subsequently, neurotransmitters activate receptors on post-neurons, resulting in postsynaptic responses.[29,30] Changes in synaptic connectivity under stimulus construct memory activity in the brain. Similarly, in the Y7C peptide synaptic transistor, which is shown in Fig. 1b, voltage spikes on the bottom gate corresponding to the presynaptic spikes facilitate current responses through the channel corresponding to the excitatory postsynaptic current (EPSC). Therefore, the Y7C peptide thin film acts as a synapse between the two neurons.

Fig. 2 shows the electrical characteristics of the Y7C peptide synaptic transistor. The gate voltage sweep induced current modulation, as shown in the transfer curves. Fig. 2a shows the changes in the on-current at a gate voltage of 20 V, and voltage hysteresis at a drain current of 1 μA as a function of the gate voltage sweep rate is shown in Fig. 2b. The on-current values are 27.56 μA, 24.72 μA, and 18.32 μA at sweep rates of 1.7, 4, and 8 V s^{-1}, respectively. A slower voltage sweep was induced, and a higher current modulation was observed. Thus, the on/off current ratio reached 9.4 $\times 10^6$ at the slowest sweep rate. In addition, the voltage hysteresis values, *i.e.*, the voltage

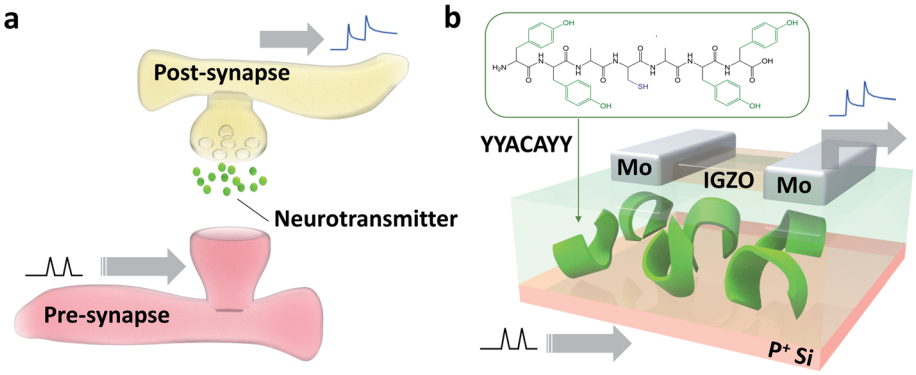

Fig. 1 Schematics of biological synapse and corresponding Y7C peptide synaptic transistor. (a) Biological communication between synapses through a synaptic cleft. Neurotransmitter is transmitted from the pre-synapse to the post-synapse, resulting in post-synaptic responses. (b) Driving mechanism of the Y7C peptide synaptic transistor. Presynaptic spikes are applied to the bottom gate electrode, and postsynaptic responses are measured at the drain electrode. Inset shows the chemical structure of the Y7C peptide.

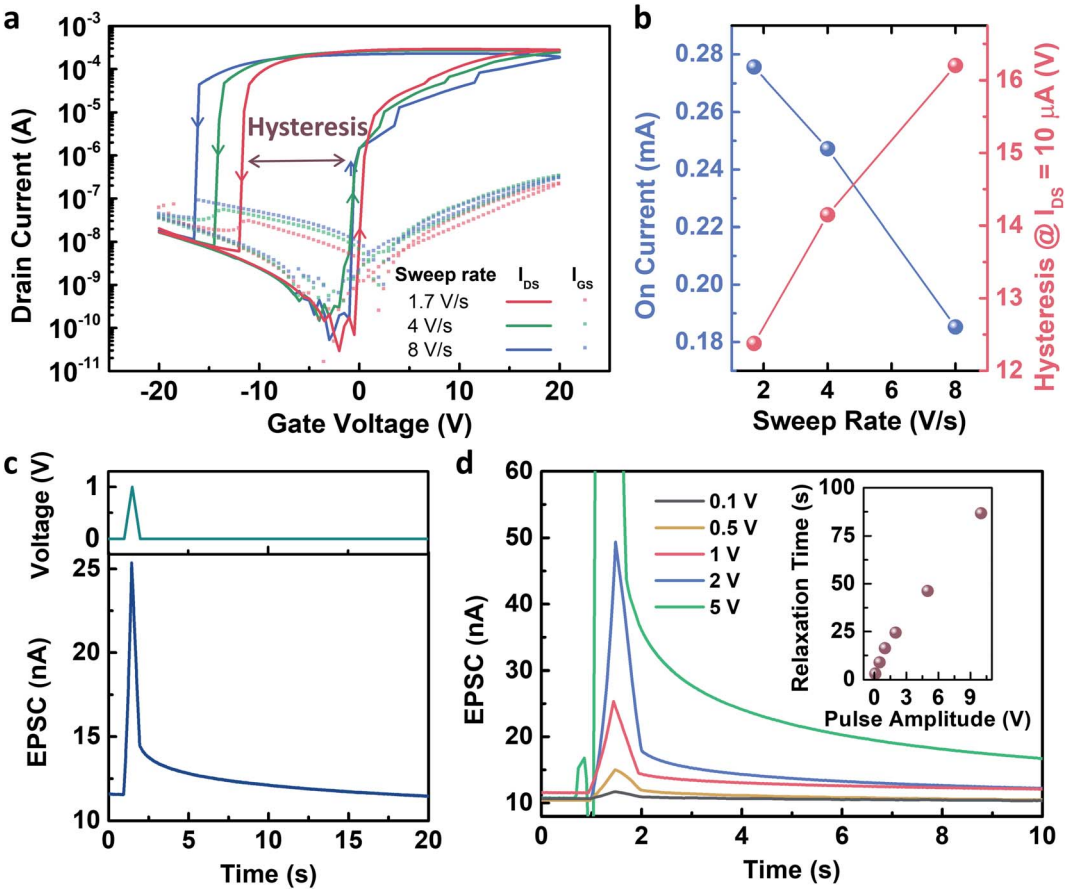

Fig. 2 Electrical characteristics of Y7C peptide synaptic transistor. (a) Transfer characteristics under 1 V drain voltage. The arrows indicate sweep directions. (b) On-current (blue) and hysteresis (red) as a function of the sweep rate of transfer curves. On-current values are measured at a gate voltage of 20 V. Voltage hysteresis is calculated as the difference between voltage values at a drain current of 10 μA during forward and reverse sweep. (c) Presynaptic spike (top) and corresponding excitatory postsynaptic current (EPSC) (bottom). (d) Pulse amplitude dependency on the EPSCs. Inset shows the relaxation time, defined as the time required to return to the original current value after stimulus.

differences between the forward and reverse sweeps at which the drain current equals 10 μA, are 12.38 V, 14.15 V, and 16.2 V at sweep rates of 1.7 V s^{-1}, 4 V s^{-1}, and 8 V s^{-1}, respectively. A large hysteresis, which increases as the sweep rate increases, indicates that ionic movement in the peptide film is the origin of the gating effect.[31] This result corresponds to our previous results from the electrochemical impedance analysis of the peptide-insulating layer.[32] The response of the transfer curves to repeated gate sweeps is shown in Fig. S3.† Therefore, a presynaptic spike induced a decay curve of the EPSC, as shown in Fig. 2c. This decaying property corresponds to the history-dependent output, resulting in the emulation of synaptic plasticity. As the amplitude of the presynaptic spikes increased, the EPSC decay slowed (Fig. 2d). Thus, the relaxation time after the stimulus increased almost linearly with the spike amplitudes. This indicates that the short-term plasticity of the device changes to long-term plasticity depending on the amplitude of the spikes. Thus, the memory property of the device can be modulated by controlling the amplitude of the stimuli, which is an important characteristic of spiking neural networks.

Several reports have shown that the accumulation of protons under the channel region induces electrostatic effects, enabling carrier generation in the channel.[31,33–35] The Y7C peptides exhibit high proton conductivity, compared to the other peptides, owing to the phenolic OH groups in tyrosine that act

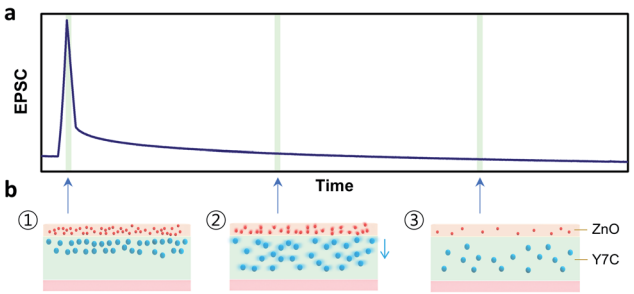

Fig. 3 Mechanism proton-induced potentiation and decay in the Y7C peptide synaptic transistor. (a) Proton accumulation-induced carrier generation and excitatory postsynaptic current. Generated current decays with time and is restored to the initial value as accumulated protons are dissipated in the Y7C film. (b) (1) Accumulation of protons near the channel/Y7C interface as a response to gate input. (2) Dissipation and diffusion of protons after removal of input stimulus. (3) Recovery to the initial state before the input stimulus. Red dots and blue dots indicate electrons and protons, respectively.

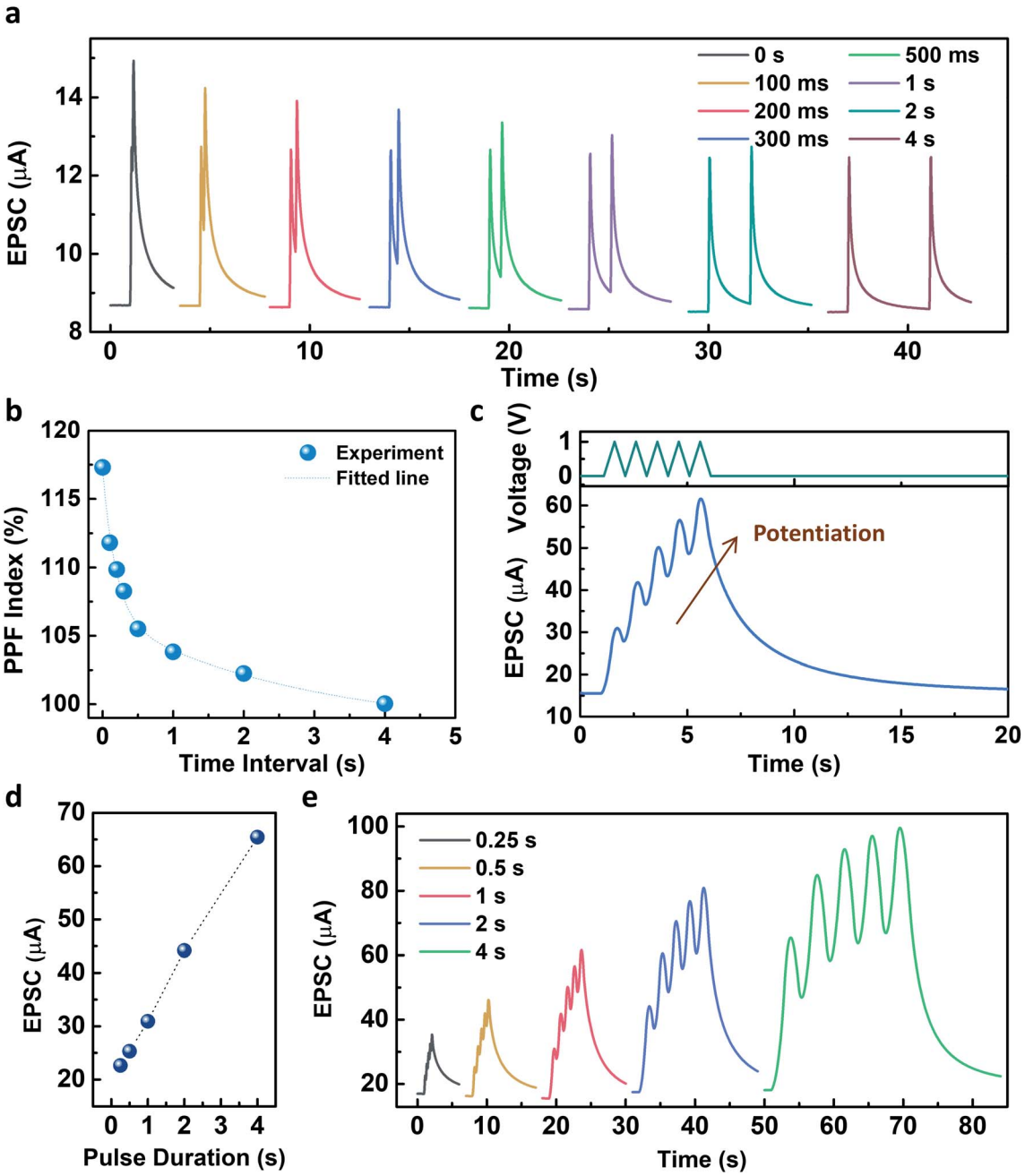

Fig. 4 Synaptic behaviors of the Y7C synaptic transistor. (a) EPSCs stimulated by paired pulses with different interval times from 0 s to 4 s. The amplitude and duration of the presynaptic spikes are 1 V and 100 ms, respectively. (b) PPF index as a function of the time interval between paired pulses. (c) Five consecutive presynaptic pulses (top) and the corresponding potentiation of the EPSCs (bottom). The amplitude and duration of the spikes are 1 V and 1 s, respectively. (d) Pulse duration dependency on the EPSCs. (e) EPSCs stimulated by 5 consecutive presynaptic pulses at different pulse durations.

as hopping sites for protons and their structural stability from disulfide bonding.[22,27] Fig. 3 shows the mechanism of proton-induced gating phenomenon in the Y7C peptide film. When a positive gate bias is applied to the bottom electrode, protons (*i.e.* positively charged hydrogen atoms) move upward through the Y7C peptide layer. Protons accumulate at the interface between the Y7C layer and the IGZO channel layer, thereby forming an electric double layer (EDL). Thus, carrier generation in the IGZO channel is induced, resulting in the current modulation of the device. This mechanism is analogous to the residual effects of Ca^{2+} dynamics in biological synapses.

Fig. 4 describes the EPSC responses triggered by consecutive presynaptic stimuli representing the emulation of synaptic plasticity. PPF, which denotes the amplitude ratio of the second EPSC response to the first response facilitated by two successive spikes (1 V, 100 ms), was investigated at various time intervals,

as shown in Fig. 4a. It was observed that the PPF gradually decreased as the time interval increased. The PPF index, defined as A_2/A_1 (%), as a function of the time interval, was fitted by using a double exponential decay curve:

$$\mathrm{PPF} = A_1 \exp\left(-x/\tau_1\right) + A_2 \exp\left(-x/\tau_2\right) + 100\ (\%)$$

where x is the interval time; A_1 and A_2 are the initial magnitudes of the rapid and slow phases, respectively; and τ_1 and τ_2 denote the characteristic relaxation times of the respective phases. The fitting shown in Fig. 4b yields $A_1 = 9.26\%$, $A_2 = 7.9\%$, $\tau_1 = 161.57$ ms, and $\tau_2 = 1398.78$ ms. The PPF results suggest that the consecutive stimuli facilitate EPSC. Furthermore, five successive presynaptic pulses (1 V, 1 s) induced a gradual increase in the EPSC amplitude corresponding to potentiation of the synaptic connectivity, as shown in Fig. 4c. The response of the synaptic response to repeated presynaptic pulses is shown in Fig. S4.†

The pulse duration dependency on the facilitation of the EPSC was further investigated with a voltage amplitude of 1 V. As shown in Fig. 4d, the facilitation of EPSC increased as the pulse duration increased from 0.25 s to 4 s. Five consecutive presynaptic pulses (1 V) with various pulse durations from 0.25 s to 4 s were applied to the Y7C peptide synaptic transistor (Fig. 4e). As the number of stimuli increased, the increase of the EPSC was facilitated independent of the pulse duration. The fabricated Y7C peptide synaptic transistors have analogous synaptic responses to a biological neuron. This makes the implementation of synaptic functions in an artificial device to mimic the processing system of an actual neural network.

Conclusion

In summary, our study demonstrates the brain-mimetic performance of three-terminal artificial synapses based on tyrosine-rich peptides. The Y7C peptide, designed to realize the coupling effect between protons and electrons, enabled synaptic plasticity owing to high proton conduction, in addition to low power operation. In an effort to enable its use in artificial spiking neural networks for neuromorphic computing, we explored various aspects of synaptic plasticity, including the PPF, transition from STP to LTP, and synaptic potentiation. Our findings highlight the material potential of the peptide for novel processors and also provide a new strategy for designing proton-based electronics by using tyrosine as a design motif.

Conflicts of interest

There are no conflicts to declare.

Acknowledgements

This work was supported by the National Research Foundation of Korea (NRF) grant funded by the Korea government (MSIT) (No. 2020R1A2C2004864).

References

1 Y. LeCun, Y. Bengio and G. Hinton, *Nature*, 2015, **521**, 436–444.
2 Y. He, L. Zhu, Y. Zhu, C. Chen, S. Jiang, R. Liu, Y. Shi and Q. Wan, *Adv. Intell. Syst.*, 2021, 2000210.
3 S. W. Cho, S. M. Kwon, Y.-H. Kim and S. K. Park, *Adv. Intell. Syst.*, 2021, 2000162.
4 Z. Wang, H. Wu, G. W. Burr, C. S. Hwang, K. L. Wang, Q. Xia and J. J. Yang, *Nat. Rev. Mater.*, 2020, **5**, 173–195.
5 M. A. Zidan, J. P. Strachan and W. D. Lu, *Nat. Electron.*, 2018, **1**, 22–29.
6 Q. Xia and J. J. Yang, *Nat. Mater.*, 2019, **18**, 309–323.
7 S. Yu, *Proc. – IEEE*, 2018, **106**, 260–285.
8 Y. van De Burgt, A. Melianas, S. T. Keene, G. Malliaras and A. Salleo, *Nat. Electron.*, 2018, **1**, 386–397.
9 E. J. Fuller, S. T. Keene, A. Melianas, Z. Wang, S. Agarwal, Y. Li, Y. Tuchman, C. D. James, M. J. Marinella and J. J. Yang, *Science*, 2019, **364**, 570–574.
10 E. J. Fuller, F. E. Gabaly, F. Léonard, S. Agarwal, S. J. Plimpton, R. B. Jacobs-Gedrim, C. D. James, M. J. Marinella and A. A. Talin, *Adv. Mater.*, 2017, **29**, 1604310.
11 H. Kim, S. Hwang, J. Park and B.-G. Park, *Nanotechnology*, 2017, **28**, 405202.
12 H. Kim, S. Hwang, J. Park, S. Yun, J.-H. Lee and B.-G. Park, *IEEE Electron Device Lett.*, 2018, **39**, 630–633.
13 L. Q. Zhu, C. J. Wan, L. Q. Guo, Y. Shi and Q. Wan, *Nat. Commun.*, 2014, **5**, 1–7.
14 S. Wang, C. Chen, Z. Yu, Y. He, X. Chen, Q. Wan, Y. Shi, D. W. Zhang, H. Zhou and X. Wang, *Adv. Mater.*, 2019, **31**, 1806227.
15 J. Shi, S. D. Ha, Y. Zhou, F. Schoofs and S. Ramanathan, *Nat. Commun.*, 2013, **4**, 1–9.
16 S. Kim, J. Yoon, H.-D. Kim and S.-J. Choi, *ACS Appl. Mater. Interfaces*, 2015, **7**, 25479–25486.
17 X. Daura, K. Gademann, B. Jaun, D. Seebach, W. F. Van Gunsteren and A. E. Mark, *Angew. Chem., Int. Ed.*, 1999, **38**, 236–240.
18 K. Tao, P. Makam, R. Aizen and E. Gazit, *Science*, 2017, **358**, eaam9756.
19 N. Ashkenasy, W. S. Horne and M. R. Ghadiri, *Small*, 2006, **2**, 99–102.
20 J. Lee, M. Ju, O. H. Cho, Y. Kim and K. T. Nam, *Adv. Sci.*, 2019, **6**, 1801255.
21 L. Hammarström and S. Styring, *Energy Environ. Sci.*, 2011, **4**, 2379–2388.
22 J. Lee, I. R. Choe, Y. O. Kim, S. D. Namgung, K. Jin, H. Y. Ahn, T. Sung, J. Y. Kwon, Y. S. Lee and K. T. Nam, *Adv. Funct. Mater.*, 2017, **27**, 1702185.
23 H.-S. Jang, J.-H. Lee, Y.-S. Park, Y.-O. Kim, J. Park, T.-Y. Yang, K. Jin, J. Lee, S. Park and J. M. You, *Nat. Commun.*, 2014, **5**, 1–11.
24 M. Ju, O. H. Cho, J. Lee, S. D. Namgung, M.-K. Song, M. Balamurugan, J.-Y. Kwon and K. T. Nam, *Phys. Chem. Chem. Phys.*, 2020, **22**, 7537–7545.

25 M.-K. Song, S. D. Namgung, T. Sung, A.-J. Cho, J. Lee, M. Ju, K. T. Nam, Y.-S. Lee and J.-Y. Kwon, *ACS Appl. Mater. Interfaces*, 2018, **10**, 42630–42636.
26 S. D. Namgung, M. K. Song, T. Sung, O. H. Cho, M. Ju, H. Kim, Y. S. Lee, K. T. Nam and J. Y. Kwon, *Adv. Mater. Technol.*, 2020, **5**, 2000516.
27 M.-K. Song, S. D. Namgung, D. Choi, H. Kim, H. Seo, M. Ju, Y. H. Lee, T. Sung, Y.-S. Lee and K. T. Nam, *Nat. Commun.*, 2020, **11**, 1–8.
28 M. Sjödin, S. Styring, H. Wolpher, Y. Xu, L. Sun and L. Hammarström, *J. Am. Chem. Soc.*, 2005, **127**, 3855–3863.
29 R. S. Zucker and W. G. Regehr, *Annu. Rev. Physiol.*, 2002, **64**, 355–405.
30 G.-q. Bi and M.-m. Poo, *J. Neurosci.*, 1998, **18**, 10464–10472.
31 Y. H. Liu, L. Qiang Zhu, Y. Shi and Q. Wan, *Appl. Phys. Lett.*, 2014, **104**, 133504.
32 T. Sung, S. D. Namgung, J. Lee, I. R. Choe, K. T. Nam and J.-Y. Kwon, *RSC Adv.*, 2018, **8**, 34047–34055.
33 L. Q. Zhu, C. J. Wan, P. Q. Gao, Y. H. Liu, H. Xiao, J. C. Ye and Q. Wan, *ACS Appl. Mater. Interfaces*, 2016, **8**, 21770–21775.
34 G. Wu, J. Zhang, X. Wan, Y. Yang and S. Jiang, *J. Mater. Chem. C*, 2014, **2**, 6249–6255.
35 L. Q. Guo, J. Wen, L. Q. Zhu, Y. M. Fu and H. Xiao, *IEEE Electron Device Lett.*, 2017, **38**, 1248–1251.